Magnetotelluric Inversion for Anisotropic Conductivities

Josef Pek[1] and Fernando A. M. Santos[2]

[1]Geophysical Institute, Academy of Sciences of the Czech Republic
Boční II/1401, CZ-14131 Prague 4–Spořilov, Czech Republic
(e-mail: jpk@ig.cas.cz)

[2]Physics Department–CGUL–University of Lisbon
Campo Grande, C8, Piso 6, 1749-016 Lisbon, Portugal
(e-mail: dfams@fc.ul.pt)

Abstract

Several versions of the magnetotelluric inversion for layered anisotropic conductors are presented. Basics of the direct problem solution and evaluation of the parametric sensitivities for anisotropic layered models are summarized. Standard linearized Occam algorithms are tested with various regularization strategies, both quadratic and non-smooth, and numerical performance of the inverse procedures is discussed. An example of a global probabilistic inference by the Markov chain Monte Carlo approach is presented, aiming at appraising the equivalencies and ambiguities characteristic for the inversion in anisotropic structures.

1 Introduction

Recent progress in the geoelectrical induction studies has established the electrical anisotropy in deeper parts of the Earth a real and significant factor of the Earth's internal structure. Though arguments have been still going on as regards possibilities to distinguish between effects of anisotropy and those produced by lateral conductivity changes or local distortions, several well-grounded studies have proved the electrical anisotropy to be fully justified within particular geological and tectonic settings (e.g., Mareschal *et al.*, 1995; Eisel and Haak, 1999). Moreover, they also have proved the electrical anisotropy to create a significant link between geoelectrical models and geodynamical interpretations.

The interpretation value of electrically anisotropic Earth structures has induced an increased interest to new interpretation methodologies for anisotropic conductors. As compared to isotropic settings, inversion for anisotropic electrical conductivities in the Earth has to deal with substantially increased number of variables, with ambiguities and equivalencies between the parameters, and also with the fact that the anisotropic Earth's structures often contradict the smoothness concept of most of the Occam-based inversion procedures.

First attempts to invert magnetotelluric (MT) data for 1-D anisotropic conductivities have been made by Abramovici and Shoham (1977), and more recently by Regis and Rijo (1997, 2000) and Santos and Mendes-Victor (1997). Abramovici and Shoham based their inversion procedure on the generalized inversion technique. Regis and Rijo use the same inversion procedure, they propose, however, to employ additional prior information from well logging and other geophysical and geological knowledge to impose constraints on the model. Santos and Mendes-Victor use the simulated annealing algorithm and consider a layered earth containing dipping anisotropy.

In this paper we concentrate on a non-linear inversion of 1-D MT anisotropic data based on the conjugate gradient and lagged diffusivity minimization. We discuss the effect of different stabilizing functionals, both quadratic and non-smooth, for the regularization of the inverse problem. Finally, we compare the inversion results with those inferred from a probabilistic Markov chain Monte Carlo method.

2 Model, Forward Solution, Parametric Sensitivities

2.1 Model of the 1-D MT Problem for Anisotropic Conductors

Throughout this paper, we will assume a simple Cagniard-Tichonov 1-D MT model extended to anisotropic layered media. The conductive structure (earth) consists of homogeneous horizontal layers with thicknesses h_l, $l = 1, \ldots, N$. The stack of layers is underlain by a homogeneous conductive halfspace. The electrical conductivity in each of the layers, as well as in the basement, is given by a conductivity tensor $\boldsymbol{\sigma}_l$, $l = 1, \ldots, N, N+1$. We

assume that $\boldsymbol{\sigma}$ is a symmetric and positive definite tensor anywhere within the earth. The halfspace above the earth is filled with perfectly insulating air, i.e. $\sigma_0 = 0$.

The earth's surface defines the xy plane of a cartesian coordinate system, the z axis is directed down into the conductive medium. The electromagnetic field is excited by a primary electromagnetic plane wave that originates from sources at $z = -\infty$ and propagates perpendicularly towards the earth's surface.

Within each layer, the conductivity tensor $\boldsymbol{\sigma}$ can be, due to its symmetry, diagonalized and expressed via three principal conductivities, σ_1, σ_2, σ_3, and a rotation matrix, which can be, in turn, decomposed into three elementary Euler's rotations, successively by angles α_L, α_D, and α_S,

$$\boldsymbol{\sigma} = \begin{pmatrix} \sigma_{xx} & \sigma_{xy} & \sigma_{xz} \\ \sigma_{yx} & \sigma_{yy} & \sigma_{yz} \\ \sigma_{zx} & \sigma_{zy} & \sigma_{zz} \end{pmatrix} = \mathbf{R}_z(-\alpha_S)\mathbf{R}_x(-\alpha_D)\mathbf{R}_z(-\alpha_L) \begin{pmatrix} \sigma_1 & 0 & 0 \\ 0 & \sigma_2 & 0 \\ 0 & 0 & \sigma_3 \end{pmatrix} \mathbf{R}_z(\alpha_L)\mathbf{R}_x(\alpha_D)\mathbf{R}_z(\alpha_S),$$

where $\mathbf{R}_x$ and $\mathbf{R}_z$ are elementary rotation matrices around the coordinate axis x and z, respectively. According to their physical relation to the anisotropy, the angles α_S, α_D, α_L can be identified with the anisotropy strike, dip, and slant, respectively.

Considering the symmetry of the above MT model, i.e. $\partial/\partial x = \partial/\partial y \equiv 0$, Maxwell's equations in each of the homogeneous subdomains of the model for a frequency ω reduce to

$$\begin{aligned} \frac{\partial E_x}{\partial z} &= i\omega\mu_0 H_y, \qquad \frac{\partial H_y}{\partial z} = -J_x = -\sigma_{xx}E_x - \sigma_{xy}E_y - \sigma_{xz}E_z, \\ \frac{\partial E_y}{\partial z} &= -i\omega\mu_0 H_x, \quad \frac{\partial H_x}{\partial z} = J_y = \sigma_{yx}E_x + \sigma_{yy}E_y + \sigma_{yz}E_z. \end{aligned} \tag{2.1}$$

The last pair of governing field equations degenerates to

$$H_z = 0, \qquad J_z = \sigma_{zx}E_x + \sigma_{zy}E_y + \sigma_{zz}E_z = 0, \tag{2.2}$$

expressing simply the absence of a vertical magnetic field and of vertical electric currents anywhere in an anisotropic layered medium.

Eliminating, e.g., the magnetic field components from (2.1), we easily arrive at a system of coupled second-order differential equations for the electric field,

$$\frac{\partial^2 E_x}{\partial z^2} + i\omega\mu_0(A_{xx}E_x + A_{xy}E_y) = 0, \qquad \frac{\partial^2 E_y}{\partial z^2} + i\omega\mu_0(A_{yx}E_x + A_{yy}E_y) = 0, \tag{2.3}$$

where

$$A_{xx} = \sigma_{xx} - \frac{\sigma_{xz}\sigma_{zx}}{\sigma_{zz}}, \quad A_{xy} = \sigma_{xy} - \frac{\sigma_{xz}\sigma_{zy}}{\sigma_{zz}}, \quad A_{yx} = \sigma_{yx} - \frac{\sigma_{yz}\sigma_{zx}}{\sigma_{zz}}, \quad A_{yy} = \sigma_{yy} - \frac{\sigma_{yz}\sigma_{zy}}{\sigma_{zz}}, \tag{2.4}$$

with clearly $A_{xy} = A_{yx}$ for a symmetric conductivity tensor $\boldsymbol{\sigma}$.

From (2.1) and the system (2.3) we can conclude that the MT field in a layered anisotropic medium depends on the elements of the conductivity tensor through the aggregate conductivities A_{xx}, A_{yy}, and A_{xy} only. Whatever the particular form of the conductivity tensor $\boldsymbol{\sigma}$, the electromagnetic field does not change if the elements of the 2×2 matrix $\mathbf{A}$ remain unchanged. Consequently, without any additional information available, the MT field of a plane wave does not allow us to reconstruct the full conductivity tensor in a 1-D medium. Only the elements of $\mathbf{A}$ can be resolved, which thus represents an equivalent effective conductivity tensor attributed to the individual layers of the model.

It can be easily shown that $\det \mathbf{A} = \det \boldsymbol{\sigma}/\sigma_{zz} > 0$. Consequently, $\mathbf{A}$ is a symmetric and positive definite 2×2 matrix, which can be again factorized in terms of its principal elements, say A_1 and A_2, and an elementary rotation, by an effective strike angle β_S, around the z coordinate axis,

$$\begin{pmatrix} A_{xx} & A_{xy} \\ A_{yx} & A_{yy} \end{pmatrix} = \begin{pmatrix} \cos\beta_S & -\sin\beta_S \\ \sin\beta_S & \cos\beta_S \end{pmatrix} \begin{pmatrix} A_1 & 0 \\ 0 & A_2 \end{pmatrix} \begin{pmatrix} \cos\beta_S & \sin\beta_S \\ -\sin\beta_S & \cos\beta_S \end{pmatrix},$$

which gives

$$A_{xx} = A_1\cos^2\beta_S + A_2\sin^2\beta_S, \quad A_{yy} = A_1\sin^2\beta_S + A_2\cos^2\beta_S, \quad A_{xy} = A_{yx} = (A_1 - A_2)\sin\beta_S\cos\beta_S.$$

Summarizing the above steps, we conclude that the 1-D MT problem for a generally anisotropic layered medium can be always re-formulated as a simpler, but equivalent problem for an azimuthally (horizontally) anisotropic structure with the horizontal conductivity tensor $\mathbf{A}$ defined by (2.4). Any changes in the full conductivity tensor $\boldsymbol{\sigma}$ that do not affect the elements of $\mathbf{A}$ cannot be recognized by MT soundings with a plane wave source field.

2.2 Principles of the Forward Solution

In the past 30 years, the solution to the 1-D direct MT problem for anisotropic structures has been presented in various forms by a number of authors (e.g., O'Brien and Morrison, 1967; Reddy and Rankin, 1971; Loewenthal and Landisman, 1973; Abramovici, 1974; Dekker and Hastie, 1980). Therefore, we will only briefly summarize the principal points of the direct solution here. For a detailed description of the problem, both theoretical and algorithmic, we refer the reader to (Pek and Santos, 2002)

The system (2.3) has the form of coupled pendula equations. Seeking the general solution to equations (2.3) in the form $\exp(\pm kz)$, we easily find that there are always two solution modes in the anisotropic medium, corresponding to two different wave numbers,

$$k_{1,2}^2 = -\frac{i\omega\mu_0}{2}\left[A_{xx} + A_{yy} \pm \sqrt{(A_{xx} - A_{yy})^2 + 4A_{xy}A_{yx}}\right].$$

In terms of the principal effective conductivities, A_1 and A_2, these wave numbers are expressed as

$$k_{1,2}^2 = -\frac{i\omega\mu_0}{2}\left(A_1 + A_2 \pm |A_1 - A_2|\right) = -i\omega\mu_0 \begin{Bmatrix}\max\\ \min\end{Bmatrix}\{A_1, A_2\} = -i\omega\mu_0 A_{1,2},$$

the last identity being true only if $A_1 \geq A_2$. This can be, however, always achieved by properly choosing the effective strike β_S. By changing β_S by $\pm 90°$, we can simply swap the principal conductivities A_1 and A_2.

Thus, two pairs of downgoing and upgoing waves exist in a generally anisotropic layer, the first one, corresponding to the wave number k_1, slow, and the other one (k_2) fast. A standard matrix propagation method can be now used to propagate the fields between different depths within the model.

For a particular z within an l-th layer, the horizontal field components can be expressed in a matrix form,

$$\mathbf{F}_l(z,\omega) = \mathbf{M}_l(z,\omega)\,\mathbf{D}_l, \qquad z \in (z_{l-1}, z_l), \quad l = 1, \ldots, N+1, \tag{2.5}$$

where $\mathbf{F}^T = (\mathbf{E}_h^T, \mathbf{H}_h^T) = (E_x, E_y, H_x, H_y)$, and $\mathbf{M}$ is a 4×4 matrix containing the exponential terms of the partial waves within the l-th layer, as well as scaling factors for the individual field components. The explicit form of the matrix $\mathbf{M}$ can be found in (Pek and Santos, 2002). The vector $\mathbf{D}$ involves four arbitrary constants which define the amplitudes of the individual partial waves within the layer considered. Within the homogeneous basement, $z > z_N$, only two of those constants which correspond to the downgoing wave modes can be non-zero for energetic reasons.

The multiplicative constants in $\mathbf{D}$ can be determined by using the general continuity conditions on the layer boundaries,

$$\mathbf{F}_l(z_l,\omega) = \mathbf{F}_{l+1}(z_l,\omega) \quad \Rightarrow \quad \mathbf{D}_l = \mathbf{M}_l^{-1}(z_l,\omega)\,\mathbf{M}_{l+1}(z_l,\omega)\,\mathbf{D}_{l+1}, \quad l = 0, \ldots, N.$$

Consequently, the field within the l-th layer can be written in the form

$$\mathbf{F}_l(z,\omega) = \mathbf{S}_l(z_l - z,\omega) \prod_{j=l+1}^{N} \mathbf{S}_j(h_j,\omega)\,\mathbf{D}_{N+1}, \qquad z \in (z_{l-1}, z_l), \tag{2.6}$$

where $\mathbf{S}_j(h_j,\omega) = \mathbf{M}_j(z_{j-1},\omega)\,\mathbf{M}_j^{-1}(z_j,\omega)$, and $h_j = z_j - z_{j-1}$. Equation (2.6) contains only two arbitrary constants from the homogeneous basement, which can be determined, e.g., by normalizing two of the four field components on the earth's surface.

Equation (2.6) allows us to recompute the electromagnetic field from the basement of the model through its layers towards the earth's surface. It represents the mathematical basis of the matrix propagation procedure for the fields in a 1-D anisotropic layered medium (e.g., O'Brien and Morrison, 1967; Loewenthal and Landisman, 1973).

The 4×4 matrices $\mathbf{S}(h,\omega)$ in (2.6) can be computed directly from the corresponding matrices $\mathbf{M}$, and can be factorized into four logical blocks,

$$\mathbf{S}(h,\omega) = \begin{pmatrix} \mathbf{S}^{EE}(h,\omega) & \mathbf{S}^{EH}(h,\omega) \\ \mathbf{S}^{HE}(h,\omega) & \mathbf{S}^{HH}(h,\omega) \end{pmatrix} = \begin{pmatrix} \mathbf{R}(-\beta_S)\,\mathbf{S}_0^{EE}(h,\omega)\,\mathbf{R}(\beta_S) & \mathbf{R}(-\beta_S)\,\mathbf{S}_0^{EH}(h,\omega)\,\mathbf{R}(\beta_S) \\ \mathbf{R}(-\beta_S)\,\mathbf{S}_0^{HE}(h,\omega)\,\mathbf{R}(\beta_S) & \mathbf{R}(-\beta_S)\,\mathbf{S}_0^{HH}(h,\omega)\,\mathbf{R}(\beta_S) \end{pmatrix},$$

where $\mathbf{R}(\beta)$ is a rotation in the (x,y)-plane by β, and the zero-indexed $\mathbf{S}$-blocks are given by

$$\mathbf{S}_0^{EE}(h,\omega) = \begin{pmatrix} \cosh k_1 h & 0 \\ 0 & \cosh k_2 h \end{pmatrix}, \qquad \mathbf{S}_0^{EH}(h,\omega) = \begin{pmatrix} 0 & \zeta_1 \sinh k_1 h \\ -\zeta_2 \sinh k_2 h & 0 \end{pmatrix},$$

$$\mathbf{S}_0^{HE}(h,\omega) = \begin{pmatrix} 0 & -\zeta_2^{-1} \sinh k_2 h \\ \zeta_1^{-1} \sinh k_1 h & 0 \end{pmatrix}, \qquad \mathbf{S}_0^{HH}(h,\omega) = \begin{pmatrix} \cosh k_2 h & 0 \\ 0 & \cosh k_1 h \end{pmatrix},$$

where $\zeta_{1,2} = -i\omega\mu_0/k_{1,2} = \sqrt{-i\omega\mu_0/A_{1,2}} = k_{1,2}/A_{1,2}$ are elementary half-space impedances for the electrical parameters of the current anisotropic layer.

The matrix expression (2.6) can be used to derive generalized recurrent formulae for recomputing the MT impedances between the boundaries of the anisotropic layers. Considering in particular the top and the bottom of the l-th layer, $z = z_{l-1}$ and $z = z_l$ respectively, we easily have a relation between the respective horizontal fields, $\mathbf{F}_{l-1}(z_l, \omega) = \mathbf{S}_l(h_l, \omega)\,\mathbf{F}_l(z_l, \omega)$. After introducing the impedance tensor by $\mathbf{E}_h(z, \omega) = \mathbf{Z}(z, \omega)\,\mathbf{H}_h(z, \omega)$, we further obtain a system of matrix equations

$$\mathbf{Z}_{l-1}\,\mathbf{H}_{h,l-1} = (\mathbf{S}_l^{EE}\,\mathbf{Z}_l + \mathbf{S}_l^{EH})\mathbf{H}_{h,l}, \qquad \mathbf{H}_{h,l-1} = (\mathbf{S}_l^{HE}\,\mathbf{Z}_l + \mathbf{S}_l^{HH})\mathbf{H}_{h,l},$$

and, consequently,

$$\mathbf{Z}_{l-1} = (\mathbf{S}_l^{EE}\,\mathbf{Z}_l + \mathbf{S}_l^{EH})(\mathbf{S}_l^{HE}\,\mathbf{Z}_l + \mathbf{S}_l^{HH})^{-1}, \tag{2.7}$$

where $\mathbf{Z}_l \equiv \mathbf{Z}(z_l, \omega)$ and $\mathbf{H}_{h,l} \equiv \mathbf{H}_h(z_l, \omega)$. When used recurrently, equation (2.7) can be used to recompute the impedance tensor from the top of the homogeneous basement up to the earth's surface. The starting tensor on the top of the homogeneous anisotropic halfspace is given by

$$\mathbf{Z}_N = -\frac{1}{2}\begin{pmatrix} -(\zeta_1 - \zeta_2)\sin 2\beta_S & (\zeta_1 + \zeta_2) + (\zeta_1 - \zeta_2)\cos 2\beta_S \\ -(\zeta_1 + \zeta_2) + (\zeta_1 - \zeta_2)\cos 2\beta_S & (\zeta_1 - \zeta_2)\sin 2\beta_S \end{pmatrix},$$

with ζ_1, ζ_2, β_S being now the halfspace parameters, i.e. $\zeta_1 \equiv \zeta_{1,N+1}$, $\zeta_2 \equiv \zeta_{2,N+1}$, and $\beta_S \equiv \beta_{S,N+1}$.

Equation (2.7) is a basis for the impedance propagation method in a 1-D anisotropic layered conductor (e.g., Abramovici, 1974; Dekker and Hastie, 1980). As in general impedances behave more regularly that the fields itself, the impedance propagation method is preferred in the numerical evaluations of the impedance tensor.

2.3 Parametric Sensitivities

Parametric sensitivities of the surface impedances with respect to the parameters of the individual layers are given by partial derivatives $\partial\mathbf{Z}(z_0, \omega)/\partial p_k$, where p_k is one of the model parameters of the k-th layer. In MT inverse applications for anisotropic 1-D conductivities/resistivities without any specific prior information on the anisotropy, it is reasonable to choose $p_k \in \{A_{1,k}, A_{2,k}, \beta_{S,k}, h_k\}$, which is a foursome of independent parameters that exhaustively characterize any anisotropic layer within a stratified medium.

The parametric sensitivities of the MT impedance for an anisotropic layered halfspace can be computed directly by differentiating the formulae (2.7) with respect to p_k. The computations simplify considerably owing to the following two facts: (i) the matrix $\mathbf{S}_l$, and consequently all its sub-blocks depend solely on the parameters of the current, i.e. the l-th layer, (ii) the MT impedance at the bottom of the l-th layer, $\mathbf{Z}_l$, does not depend on any parameter of any layer above that boundary.

From (2.7), we have generally

$$\frac{\partial\mathbf{Z}_{l-1}}{\partial p_k}(\mathbf{S}_l^{HE}\,\mathbf{Z}_l + \mathbf{S}_l^{HH}) + \mathbf{Z}_{l-1}\left(\frac{\partial\mathbf{S}_l^{HE}}{\partial p_k}\,\mathbf{Z}_l + \mathbf{S}_l^{HE}\frac{\partial\mathbf{Z}_l}{\partial p_k} + \frac{\partial\mathbf{S}_l^{HH}}{\partial p_k}\right) = \frac{\partial\mathbf{S}_l^{EE}}{\partial p_k}\,\mathbf{Z}_l + \mathbf{S}_l^{EE}\frac{\partial\mathbf{Z}_l}{\partial p_k} + \frac{\partial\mathbf{S}_l^{EH}}{\partial p_k}.$$

By virtue of the above properties, we obtain, after some simple algebra,

$$\frac{\partial\mathbf{Z}_{l-1}}{\partial p_k} = \begin{cases} \mathbf{0} & \text{if } k < l, \\ (\mathbf{R}_l^{DE}\mathbf{Z}_l + \mathbf{R}_l^{DH})\,\mathbf{R}_l^{-1} & \text{if } k = l, \\ \mathbf{R}_l^{E}\,\dfrac{\partial\mathbf{Z}_l}{\partial p_k}\,\mathbf{R}_l^{-1} & \text{if } k > l, \end{cases} \tag{2.8}$$

with the following auxiliary matrices introduced,

$$\mathbf{R}_l = \mathbf{S}_l^{HE}\,\mathbf{Z}_l + \mathbf{S}_l^{HH},\ \mathbf{R}_l^{E} = \mathbf{S}_l^{EE} - \mathbf{Z}_{l-1}\,\mathbf{S}_l^{HE},\ \mathbf{R}_l^{DE} = \frac{\partial\mathbf{S}_l^{EE}}{\partial p_k} - \mathbf{Z}_{l-1}\frac{\partial\mathbf{S}_l^{HE}}{\partial p_k},\ \mathbf{R}_l^{DH} = \frac{\partial\mathbf{S}_l^{EH}}{\partial p_k} - \mathbf{Z}_{l-1}\frac{\partial\mathbf{S}_l^{HH}}{\partial p_k}.$$

Now, by using (2.8) recurrently, we have explicitly

$$\frac{\partial\mathbf{Z}_{l-1}}{\partial p_k} = \left[\prod_{j=l}^{k-1}\mathbf{R}_j^{E}\right](\mathbf{R}_k^{DE}\mathbf{Z}_k + \mathbf{R}_k^{DH})\left[\prod_{j=l}^{k}\mathbf{R}_j\right]^{-1}. \tag{2.9}$$

Formulae (2.9) can be easily integrated into the algorithm for the direct problem solution for the impedances $\mathbf{Z}$ (Pek and Santos, 2002). Proceeding from the top of the homogeneous basement through the stack of the layers

towards the earth's surface, then for a particular, say l-th, layer, we first propagate the impedance tensor from its bottom, $\mathbf{Z}_l$, to its top, $\mathbf{Z}_{l-1}$, by using equation (2.7). Next, we compute the auxiliary matrices $\mathbf{R}_l^E$, $\mathbf{R}_l^{DE}$, and $\mathbf{R}_l^{DH}$ from the now known impedances $\mathbf{Z}_l$ and $\mathbf{Z}_{l-1}$, and from the sub-matrices of $\mathbf{S}_l$ and their derivatives with respect to p_l, the calculation of which is an elementary procedure. Then, the bottom formula in (2.8) is used to propagate all the derivatives from the deeper layers through the current layer to its top, while the middle formula in (2.8) is applied to initiate the derivatives with respect to the parameters of the current layer. In this way, we propagate both the impedance tensor and all its parametric derivatives up to the earth's surface.

Parametric sensitivities of an anisotropic layered model are a suitable tool to analyze the influence of the model parameters on the surface impedances. The sensitivity analysis can provide information as to the possibility to resolve particular features of the model from MT data. In Fig. 1 we demonstrate the parametric sensitivities for a specific model which we use in the following sections as a test model for assessing the performance of the inversion experiments. The model consists of five layers, two of which are anisotropic with different anisotropy strikes. The parameters of the model are given in the following table:

Layer	h (km)	β_S (deg)	$\varrho_{\min}$ (Ωm)	$\varrho_{\max}$ (Ωm)	$S_{\min}$ (Siemens)	$S_{\max}$ (Siemens)
1	3		1000		3	
2	7	-50	3	300	23.3	2333.3
3	60		1000		60	
4	130	20	30	300	433.3	4333.3
5	∞		200			

The difference between the directions of the preferred conductivity of the two anisotropic layers is 70 deg, and the conductances are chosen so that the deep anisotropic layer can be reliably sensed in the direction of its anisotropy strike. There are altogether 19 parameters in the model if all layers are considered anisotropic.

The gray scale maps in Fig. 1 show modules of the real and imaginary parts of the following sensitivity functions for each impedance element and for each layer,

$$s(\ln A_l) = \frac{A_l}{|Z|}\frac{\partial Z}{\partial A_l} = \frac{1}{|Z|}\frac{\partial Z}{\partial \ln A_l},\ l=1,2, \quad s(\beta_S) = \frac{1}{|Z|}\frac{\partial Z}{\partial \beta_S}, \quad s(\ln h) = \frac{h}{|Z|}\frac{\partial Z}{\partial h} = \frac{1}{|Z|}\frac{\partial Z}{\partial \ln h}, \tag{2.10}$$

which express the relative change of the particular impedance element with respect to the respective parameter, or to its logarithm in case of conductivities and thicknesses. The relative sensitivities defined in this way lead to simple sensitivity formulas for the standard MT functions, i.e., apparent resistivities ϱ^a and impedance phases φ,

$$\frac{1}{\varrho^a}\frac{\partial \varrho^a}{\partial p} = \frac{\partial \ln \varrho^a}{\partial p} = 2\,\mathrm{Re}\left[s(p)\,\frac{Z^*}{|Z|}\right], \qquad \frac{\partial \varphi}{\partial p} = \mathrm{Im}\left[s(p)\,\frac{Z^*}{|Z|}\right],$$

where asterisk is for complex conjugate. The normalized impedances, $Z/|Z|$, displayed in the top panels of Fig. 1 along with the model section, represent weighting factors for the conversion of the impedance sensitivities to the sensitivities of the MT functions.

3 Inversion

3.1 Target Function

Our approach to the MT inversion for anisotropic layered models is based on the standard Occam idea (e.g., Constable *et al.*, 1987) of minimizing the structure with the data fit used as a constraint in the minimization problem. The parametric functional to be minimized can be written in a general form

$$\Phi(\mathbf{m},\lambda) = \Phi_{\mathrm{struct}}(\mathbf{m},\mathbf{m}^{\mathrm{prior}}) + \lambda^{-1}\Phi_{\mathrm{dat}}(\mathbf{m}) \to \min, \quad \text{with } \Phi_{\mathrm{dat}}(\mathbf{m}) = \left\|\mathbf{W}_{\mathrm{D}}[\mathbf{d}^{\mathrm{mod}}(\mathbf{m}) - \mathbf{d}^{\mathrm{obs}}]\right\|^2, \tag{3.1}$$

where $\mathbf{m}$ is the vector of the model parameters, $\mathbf{m}^{\mathrm{prior}}$ contains prior estimates of the the model parameters, $\mathbf{d}^{\mathrm{obs}}$ are the measured data, $\mathbf{W}_D$ the covariance matrix of the experimental data, and $\mathbf{d}^{\mathrm{mod}}(\mathbf{m})$ is the forward solution of the MT problem for the model parameters $\mathbf{m}$. The parameter λ is a regularization parameter which specifies the weight given to the structural constraint $\Phi_{\mathrm{struct}}(\mathbf{m},\mathbf{m}^{\mathrm{prior}})$ at the expense of the data fit $\Phi_{\mathrm{dat}}(\mathbf{m})$.

In our experiments, the parametrization of the model is based on dividing the 1-D section into a logarithmically uniform system of homogeneous layers between two depth limits, which are derived from estimates of the minimum and maximum apparent penetration depths of the electromagnetic field in the medium. Then, the parameters of the model (vector $\mathbf{m}$) are the logarithms of the minimum and maximum horizontal resistivities and the direction of the minimum resistivity (anisotropy strike) within each of the layers. We have proved in Section 2.1 that these

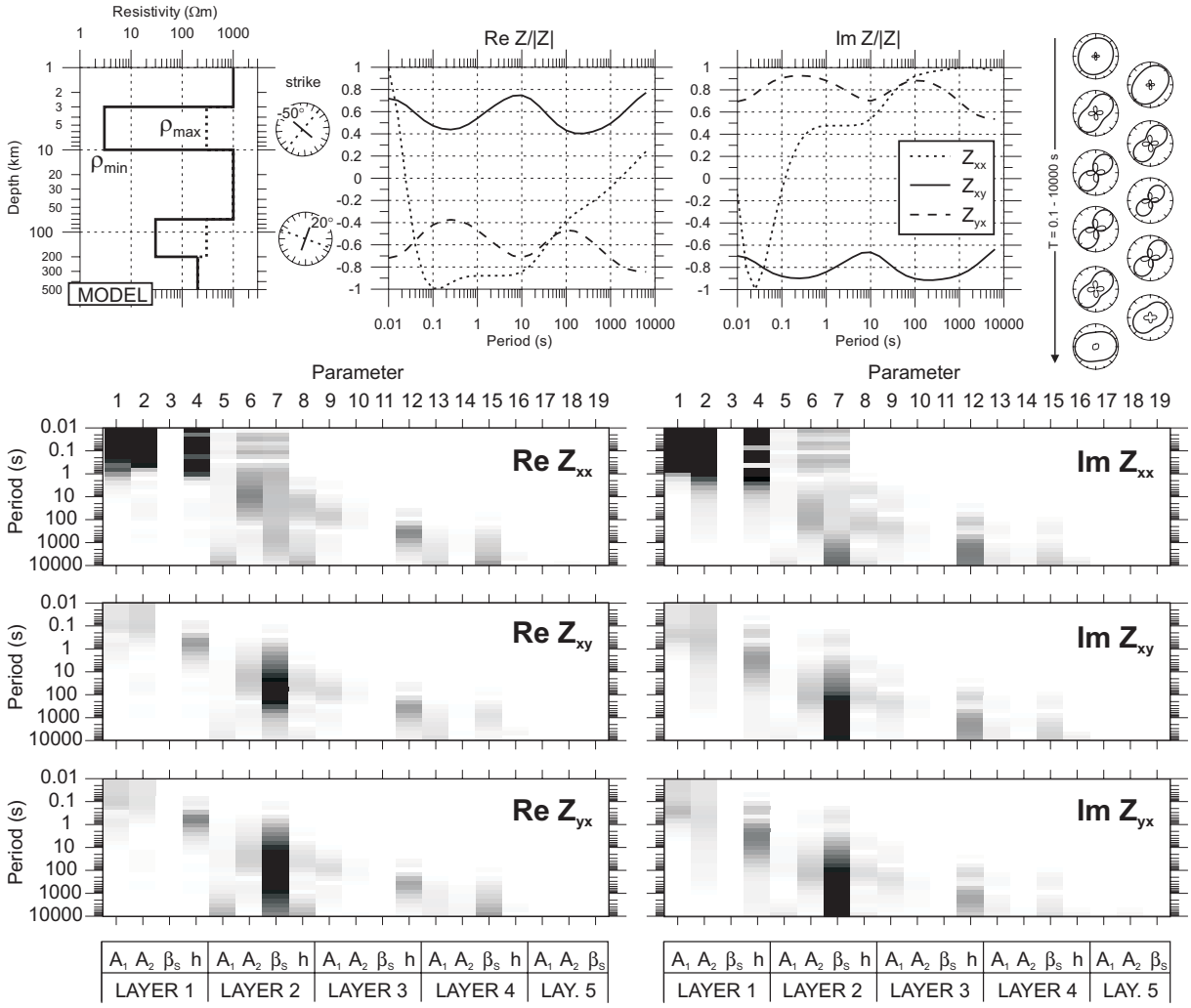

Figure 1: Modules of the normalized sensitivities (2.10) for a 5-layer anisotropic model described in the text. Top panel, left—Model section with the maximum (full line) and minimum (dashed line) resistivities and the anisotropy strikes within the individual layers. Top panel, middle—Real and imaginary parts of the normalized impedances $Z/|Z|$ within the period range of 10^{-2} to 10^4 s. Top panel, right—Polar impedance diagrams for selected periods. Bottom panels—Gray scale plots of the absolute values of the normalized parametric sensitivities (2.10) for the real and imaginary parts of the individual impedance elements as functions of period. Due to the symmetry $Z_{yy} = -Z_{xx}$, the sensitivity plot for Z_{yy} is identical with that for Z_{xx}. All layers are considered anisotropic for the sensitivity evaluations. The anisotropy strike in isotropic layers is 0 deg by default here.

parameters describe the anisotropic layer completely for MT considerations. For a fine enough sampling of the halfspace, the layer geometry (layer thicknesses) need not be included into the set of the variable parameters.

In resolving the parameters of an anisotropic conductor, the secondary (diagonal) impedances play a crucial role. Therefore, the experimetal data vector $\mathbf{d}^{\rm obs}$ is formed of the impedance elements rather than of the usual apparent resistivity and phase data.

The aim of introducing the structural penalty $\Phi_{\rm struct}(\mathbf{m}, \mathbf{m}^{\rm prior})$ is to prevent the model from showing unnecessary structural features that result from overfitting the experimental data, i.e., from fitting the noise component in the observations. The minimum norm (Tikhonov and Arsenin, 1977), minimum roughness and minimum curvature (Constable *et al.*, 1987) are the most popular structural penalties used in geoelectrical inversions, both due to their interpretation efficiency and numerical straightforwardness.

Anisotropic geoelectrical structures are, however, often connected with spatially localized geological phenomena, such as shear zones, fractured complexes, etc., which do not conform the idea of a gradual, diffuse transition to the neighbouring units. Moreover, experiments with 2-D anisotropic models have shown that interactions of largely anisotropic domains with different anisotropy directions can result in heavy distortions of the MT impedances (Pek and Verner, 1997). It is, therefore, desirable to limit both the spatial extent of the anisotropic domains and the anisotropy variations within those domains by employing modified regularization strategies which give preference to the 'non-smooth' structural features. In this study, we have tested several regularization approaches, both

Penalty	Theoretical formula	Numerical representation
Least-squares norm[1]	$\int_0^\infty [m(z) - m^{\rm prior}(z)]^2\, dz$	$\sum_i (m_i - m_i^{\rm prior})^2$
Roughness[2]	$\int_0^\infty [\nabla m(z)]^2\, dz$	$\sum_i (m_i - m_{i-1})^2$
Total variation[3]	$\int_0^\infty \lvert\nabla m(z)\rvert\, dz$	$\sum_i \sqrt{(m_i - m_{i-1})^2 + \beta^2},\ \beta \to 0$
Minimum support[4]	$\int_0^\infty \frac{[m(z)-m^{\rm prior}(z)]^2}{[m(z)-m^{\rm prior}(z)]^2+\beta^2}\, dz,\ \beta \to 0$	$\sum_i \frac{(m_i-m_i^{\rm prior})^2}{(m_i-m_i^{\rm prior})^2+\beta^2},\ \beta \to 0$
Minimum gradient support[5]	$\int_0^\infty \frac{[\nabla m(z)]^2}{[\nabla m(z)]^2+\beta^2}\, dz,\ \beta \to 0$	$\sum_i \frac{(m_i-m_{i-1})^2}{(m_i-m_{i-1})^2+\beta^2},\ \beta \to 0$

Table 1: Summary of the regularization functionals used in our inversion tests for anisotropic layered conductivities. [1](Tikhonov and Arsenin, 1977) Minimizes the LS norm of the deviation of the model from a prior distribution. [2](Constable *et al.*, 1987) Minimizes the roughness of the parameters in the LS sense. Prefers slow variations, tends to oversmooth the solution and suppress any sharp changes in the solution. [3](Rudin *et al.*, 1992) Minimizes the total variation of the parameter. It is indifferent to the size of the parameter jumps, and can preserve sharp edges in the solution. It is non-differentiable at points with zero gradient, hence introduction of a small stabilizing β is necessary. [4](Portniaguine and Zhdanov, 1999) For a sufficiently small stabilizing β, it penalizes any deviation from $m^{\rm prior}(z)$ by the same amount, independently of the size of the deviation. [5](Portniaguine and Zhdanov, 1999) For a sufficiently small stabilizing β, it penalizes any sharp change in the solution, independently of the size of the jump. Tends to produce models with a minimum number of layers.

quadratic and non-quadratic, which have recently been used in other geophysical interpretations (Portniaguine and Zhdanov, 1999). A summary of the regularization functionals used in our experiments is given in Tab. 1. We refer the reader to (Portniaguine and Zhdanov, 1999) for the mathematical background and the proof that the considered functionals are stabilizers in sense of the Tikhonov regularization theory.

One of the serious questions of the regularized inversion (3.1) is a particular choice of the regularization parameter λ. One of the popular approaches in this respect is the L-curve criterion (Hansen, 1992). The L-curve is a plot of the norm of the regularized solutions $\Phi_{\rm struct}(\mathbf{m}, \mathbf{m}^{\rm prior})$ versus the norm of the residuals $\Phi_{\rm dat}(\mathbf{m})$. This dependence has often an L-shaped form which reflects the heuristics that for large λ's the residual increases without reducing the structural norm of the solution much, while for small λ's the norm of the solutions increases rapidly without much decrease in the data residual. Thus, the best regularization parameter should lie on the corner of the L-curve. Though the L-curve approach is not flawless (see, e.g., Engel and Grever, 1994), we have used it in our experiments to estimate the quasi-optimal regularization parameter λ.

3.2 Local Minimization

Commonly, the Newton-type methods are employed for minimizing the target function (3.1), particularly if quadratic regularization is implemented (e.g., Constable *et al.*, 1987). The use of non-quadratic regularization functionals can, however, result in serious non-linearities of the target function and its derivatives, and may degrade, or even completely corrupt, the convergence of the Newton-type minimization methods.

Portniaguine and Zhdanov (1999) propose to minimize (3.1) by using the conjugate gradient reweighted optimization with line search. They minimize the target function of a particular form

$$\Phi(\mathbf{m}, \lambda) = \left\|\mathbf{W}_M(\mathbf{m})(\mathbf{m} - \mathbf{m}^{\rm prior})\right\|^2 + \lambda^{-1} \left\|\mathbf{W}_D[\mathbf{d}^{\rm mod}(\mathbf{m}) - \mathbf{d}^{\rm obs}]\right\|^2 \to \min, \tag{3.2}$$

where the specific structural norm given by the first term on the r.h.s. of (3.2) is shown to be compatible with all the regularization functions in Tab. 1. The minimization process in the iteration step $(k+1)$ is based on a line search for the minimum of $\Phi[\mathbf{m}^{(k)} - \tau \mathbf{g}(\mathbf{m}^{(k)})]$ with respect to τ, where $\mathbf{g}(\mathbf{m}^{(k)})$ is the conjugate gradient direction,

$$\mathbf{g}(\mathbf{m}^{(k)}) = \mathbf{g}_0(\mathbf{m}^{(k)}) + \gamma_k \mathbf{g}(\mathbf{m}^{(k-1)}),\ \text{with}\ \gamma_k = \|\mathbf{g}_0(\mathbf{m}^{(k)})\|^2 / \|\mathbf{g}_0(\mathbf{m}^{(k-1)})\|^2,$$

and $\mathbf{g}_0(\mathbf{m}^{(k)})$ is the gradient of (3.2) in the k-th step, with the generally non-linear matrix $\mathbf{W}_M(\mathbf{m})$ fixed with the arguments of the current iteration step, i.e., $\mathbf{m} = \mathbf{m}^{(k)}$,

$$\mathbf{g}_0(\mathbf{m}^{(k)}) = 2\, \mathbf{W}_M^T(\mathbf{m}^{(k)})\, \mathbf{W}_M(\mathbf{m}^{(k)})\, (\mathbf{m}^{(k)} - \mathbf{m}^{\rm prior}) + 2\lambda^{-1} [\mathbf{S}^{\rm mod}(\mathbf{m}^{(k)})]^T \mathbf{W}_D^T \mathbf{W}_D [\mathbf{d}^{\rm mod}(\mathbf{m}^{(k)}) - \mathbf{d}^{\rm obs}],$$

where $\mathbf{S}^{\rm mod}(\mathbf{m}) = \nabla_M [\mathbf{d}^{\rm mod}(\mathbf{m})]^T$ is a matrix of the Frechet (parametric) derivatives of the forward solution. The structural weighting matrix $\mathbf{W}_M(\mathbf{m})$ is updated on every iteration, which clarifies the reweighting character of the algorithm. The convergence of the conjugate gradient optimization has been found reliable in practical tests, with typically several tens of iteration steps required to converge to the solution for reasonable models.

Another minimization procedure we have tested here is an analogy to the lagged diffusivity method which had been earlier proposed for problems in the image processing with the total variation regularization (Vogel and Oman, 1998). Let us express the parametric gradient of the structure norm in the form $\nabla_M \Phi_{\rm struct}(\mathbf{m}) = 2\,\mathbf{W}_{MD}(\mathbf{m})(\mathbf{m}-\mathbf{m}^{\rm prior})$, which can be easily verified for all structure norms in Tab. 1. Then, the necessary condition for the target function (3.1) to reach a minimum is

$$\nabla_M \Phi(\mathbf{m},\lambda) = 2\,\lambda^{-1}[\mathbf{S}^{\rm mod}(\mathbf{m})]^T\,\mathbf{W}_D^T\,\mathbf{W}_D\,[\mathbf{d}^{\rm mod}(\mathbf{m})-\mathbf{d}^{\rm obs}] + 2\,\mathbf{W}_{MD}(\mathbf{m})\,(\mathbf{m}-\mathbf{m}^{\rm prior}) = 0, \qquad (3.3)$$

which is similar to $\mathbf{g}_0(\mathbf{m})$ above, except that now the matrix $\mathbf{W}_{MD}(\mathbf{m})$ corresponds to the exact gradient of the respective structure norm. The lagged diffusivity method consists in applying the standard Gauss-Newton optimization procedure to (3.3) with the weighting matrix $\mathbf{W}_{MD}$ kept fixed with the parameters of the current iteration step. Thus, we obtain a modified Gauss-Newton iteration process

$$\begin{aligned}\mathbf{m}^{(k+1)} = \mathbf{m}^{(k)} &- \Big\{[\mathbf{S}^{\rm mod}(\mathbf{m}^{(k)})]^T\,\mathbf{W}_D^T\,\mathbf{W}_D\,\mathbf{S}^{\rm mod}(\mathbf{m}^{(k)}) + \lambda\mathbf{W}_{MD}(\mathbf{m}^{(k)})\Big\}^{-1} \\ &\times \Big\{[\mathbf{S}^{\rm mod}(\mathbf{m}^{(k)})]^T\,\mathbf{W}_D^T\,\mathbf{W}_D\,[\mathbf{d}^{\rm mod}(\mathbf{m}^{(k)})-\mathbf{d}^{\rm obs}] + \lambda\mathbf{W}_{MD}(\mathbf{m}^{(k)})\,(\mathbf{m}^{(k)}-\mathbf{m}^{\rm prior})\Big\}. \qquad (3.4)\end{aligned}$$

The convergence of the process (3.4) is generally not guaranteed for non-linear problems, and we have encountered situations in numerical tests when the parameter correction given by (3.4) resulted in increase of the target function between successive iterations. In such a case, the correction step was divided by a factor of 2 until a decrease of the target function was achieved. With this modification, the algorithm converged reliably, with typically less than fifty iteration steps required to reach the solution.

In Fig. 2 we demonstrate the performance of the inverse solution for a synthetic data set generated from the five-layer model given in Fig. 1. For the inversion tests, the impedance values were contamined with two per cent Gaussian noise. The inverse solution was regularized by employing the standard roughness penalty. Fig. 2a shows the corresponding L-curve for various regularization parameters λ from 1 up to 30000. The values of λ in the 'knee' region of the L-curve are between about 300 and 1000. The plots in Figs. 2d, e, f show the resulting models for $\lambda = 3$ (overfitting), $\lambda = 300$ (corner of the L-curve), and $\lambda = 3000$ (oversmoothing), respectively.

Considering the model in Fig. 2e a solution to the regularized inverse problem, we see that the two anisotropic conductors of the original synthetic model are correctly recovered as to their depth range (3 to 10 km, and 70 to 200 km), and roughly also as regards the resistivity values (3 and 300 Ωm for the shallow layer, and 30 and 300 Ωm for the deep conductor). The shallow strike ($-50\,^\circ$) is recovered correctly as well, while the interpreted deep strike (about 30°) is slightly greater than the true value (20°). The most serious discrepancy between the original model and the inverse solution is excessive anisotropy, of more than one order of magnitude in terms of the resistivity ratio, between the two anisotropic conductors, which results from a poor resolution of the MT data with respect to the resistive layer (1000 Ωm) within the range of 10 to 70 km.

In the following experiments we have tried to suppress the redundant anisotropy in the structure by imposing an additional constraint on the resistivity anisotropy within the model. The particular penalty function has been chosen $\Phi_{\rm anis} = \int_0^\infty |\log[\varrho_{\max}(z)/\varrho_{\min}(z)]|\,dz$ with a weighting factor w_a. In the first step, we have fixed the weight of the roughness penalty at $\lambda = 300$, and changed only the weight of the anisotropy penalty w_a so that the product $\lambda w_a \in (1, 30000)$. In this way we could analyze how much of the anisotropy can be removed from the model in Fig. 2e without affecting the data fit much. The corresponding L-curve is displayed in Fig. 2b. The curve shows that for λw_a greater than about 200, the residual norm increases rapidly, whereas for those values below 100 the fit is practically the same as for the model without the anisotropy penalty applied. The inverse solution for $\lambda w_a = 100$ is shown in Fig. 2g.

A more objective approach is to employ both the structure and anisotropy penalty simultaneously via a multi-objective minimization procedure applied to the function

$$\Phi(\mathbf{m},\lambda,w_a) = \Phi_{\rm struct}(\mathbf{m},\mathbf{m}^{\rm prior}) + w_a\Phi_{\rm anis}(\mathbf{m}) + \lambda^{-1}\Phi_{\rm dat}(\mathbf{m}) \to \min. \qquad (3.5)$$

For this purpose, we plotted a generalized L-surface in Fig. 2c which shows the data residuals as a function of both the roughness and anisotropy penalty weights. Two models corresponding to the weights from the 'knee' region of the L-surface are presented in Figs. 2h, i, and show a relatively successful recovery of the anisotropic domains. As the periods used cover the section within the depth range of roughly 1.5 to 200 km, the excessive anisotropies in the very shallow and very deep parts of the model have no significance. Similarly, rapid jumps in the strike are a consequence of local swaps between the maximum and minimum resistivities within practically isotropic layers of the models, and have no significance.

Figs. 3 and 4 show results of analogous experiments with, respectively, the total variation and gradient support penalties. The stabilizing parameter β was chosen 0.1 in both those cases. Both approaches show a better 'de-smoothing' performance as compared with the results in Fig. 2.

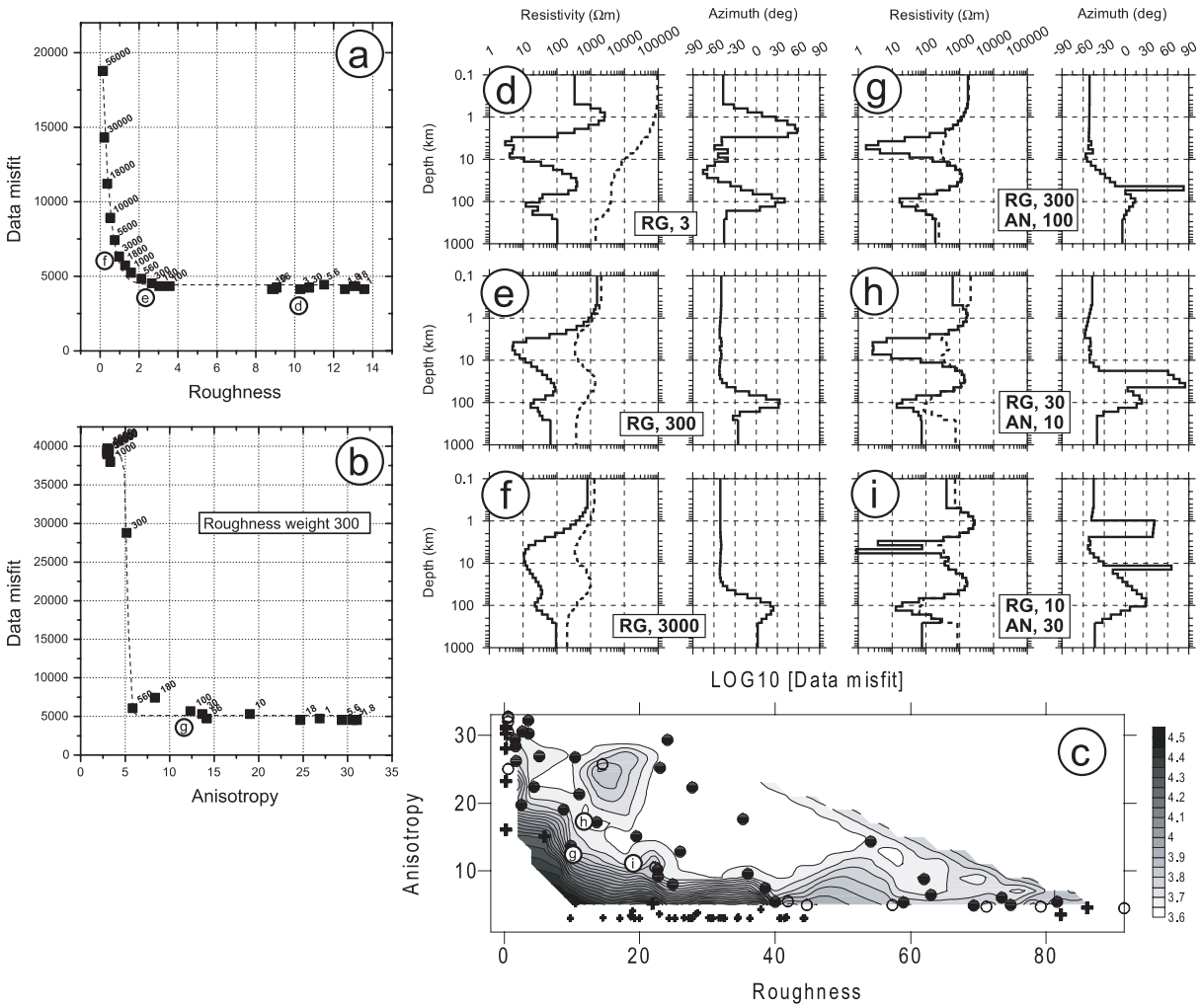

Figure 2: a—L-curve for the inversion of the synthetic data from Section 2.3, Fig. 1, with the roughness penalty employed. The models corresponding to the points d, e, and f are shown in the respective model panels to the right, which are labeled with the particular values of the regularization weights (RG, λ). b—L-curve for a fixed roughness and a variable anisotropy penalty weight. The model corresponding to the point g is shown in the respective model panel. c—L-surface for variable roughness and anisotropy penalty weights. The $(\lambda, \lambda w_a)$ points are posted on the plot and classified by shape according to the log of the corresponding data misfit (full circles < 3.8, empty circles $3.8 - 4.0$, big crosses $4.0 - 4.5$, small crosses > 4.5). Two models from the 'knee' region of the L-surface are shown as models h and i in the model panels above.

The developed algorithm has been used to practical data from MT experiments in southern Portugal, in the transition from the Southern Portuguese Zone to the Ossa Morena Zone. For the geophysical context of these MT data, as well as a discussion of the possible sources of the anisotropy, see (Santos *et al.*, 1999). Here, on an example of one site from the above experiment, we will only demonstrate some aspects of the anisotropic inversion with practical data.

First, experimental data rarely meet exactly the basic 1-D anisotropy condition, $Z_{xx} = -Z_{yy}$ (see, e.g., Abramovici, 1974; Kováčiková and Pek, 2002). The secondary impedances are generally affected by static distortions, lateral inhomogeneities, and, last but not least, they are more susceptible to noise corruption due to their small magnitudes. Fig. 5 shows the experimental data, the L-surface for the total variation and anisotropy penalties, as well as three representative models, a, b, and c, from the 'knee' region of the L-surface, ordered according to increasing/decreasing total variation/anisotropy. The inversion was carried out with both secondary impedances Z_{xx} and Z_{yy} considered in the target function, which necessarily produced models with secondary impedances fitting some average of the real secondary curves (see the full lines in the top panels of Fig. 5). Considering only one of the experimental secondary impedances, and using its mirror image for the other one, the interpretation may change, as illustrated by models in Fig. 5d (only Z_{xx} used, fit to the data shown by a dashed line in the top panels) and 5e (only Z_{yy} used, fit by a dotted line in the top panels). In this particular case, the main difference is observed in a largely anisotropic domain at about 10 km. According to the Z_{xx} data, this layer is situated in the lower crust,

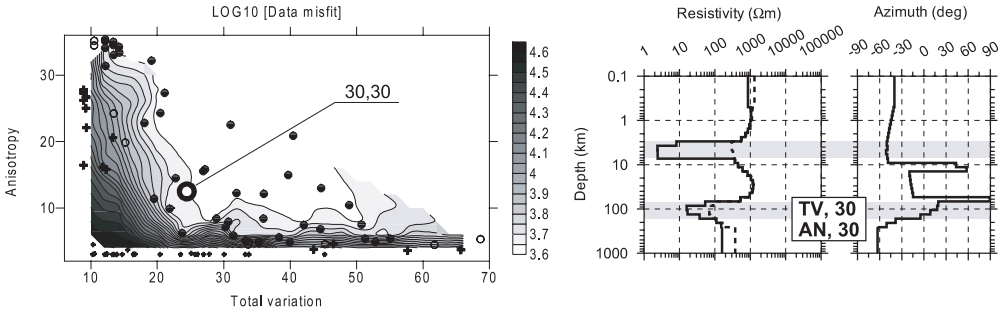

Figure 3: L-surface and a representative inverse model for the synthetic test data from Section 2.3. A multi-objective regularization with a total variation penalty and the minimum $l1$-norm anisotropy is applied.

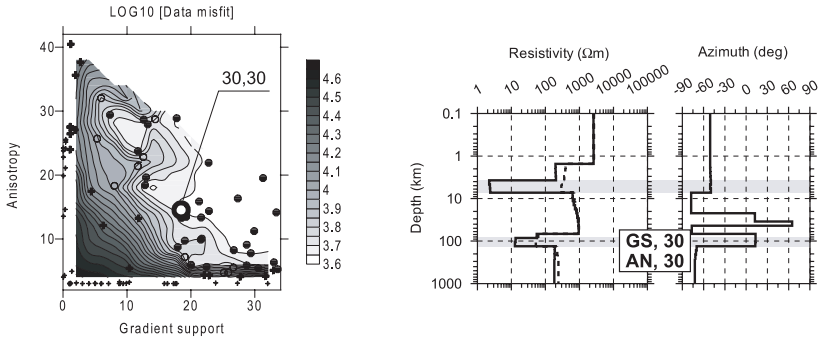

Figure 4: L-surface and a representative inverse model for the synthetic test data from Section 2.3. A multi-objective regularization with a gradient support penalty and the minimum $l1$-norm anisotropy is applied.

between roughly 10 and 20 km, is characterized by the minimum resistivity of about 2 Ωm and strike close to $\pm 90°$. From the Z_{yy} data, the anisotropic conductor is shallower, situated between about 7 and 10 km, with an extremely low minimum resistivity of less than 1 Ωm and the strike close to $-60°$.

Another effect of the anisotropic inversion is a manifestation of the anisotropy 'oversmoothing'. The differences in the models in Figs. 5a, b, c demonstrate that, though the smoothing is active in the inverse process, the anisotropy penalty used in (3.5) tends to produce largely anisotropic separated thin sheets if w_a is too large, and, thus, to add excessive structure to the model.

3.3 Global Optimization: An Example

Besides the local optimization techniques described in the preceding section, we carried out additional inversion experiments with the global optimization procedures, in particular the controlled random search (Martinez, 1988) and Markov chain Monte Carlo (MCMC) method (e.g., Neal, 1993). We only show here for comparison one result obtained from the latter procedure which can help in qualitatively assessing the significance of the inversion results from the previous experiments.

The MCMC methods represent a class of statistical inference methods that allow us to draw, in a computationally feasible way, samples from extremely complex probability distributions, and to estimate moments of functions under these distributions. In application to the inverse problems, the MCMC is used to estimate the posterior distribution of the unknown parameters conditioned on the observed data. From the posterior density, various estimates for the parameter distribution can be calculated as well as a posteriori uncertainties. A flexible formulation of the priors makes it possible to incorporate structure penalties of various character into the inference process.

As we have, for our anisotropic problem, almost exactly repeated the MCMC procedure proposed for a 1-D MT inversion by Grandis *et al.* (1999), we will not go into further methodological details here. In Fig. 6, we present an interpretation of the synthetic data set from Section 2.3, which we have also used for testing in the previous section. The gray shade plots show the marginal probability distributions for the maximum and minimum resistivities and for the anisotropy strike within individual layers of the model; the original true model is displayed as well for reference. A roughness penalty has been used to modify the prior distribution, with a regularization weight $\lambda = 3$, which corresponds to only a weak smoothing of the parameters.

The plots clearly indicate that all parameters of the shallow anisotropic layer are well resolved, especially in its upper part between 3 and 6 km. From the parameters of the deep anisotropic layer, only the minimum resistivity is well resolved at depths of about 80 to 120 km. The distribution function of the maximum resistivity and that of

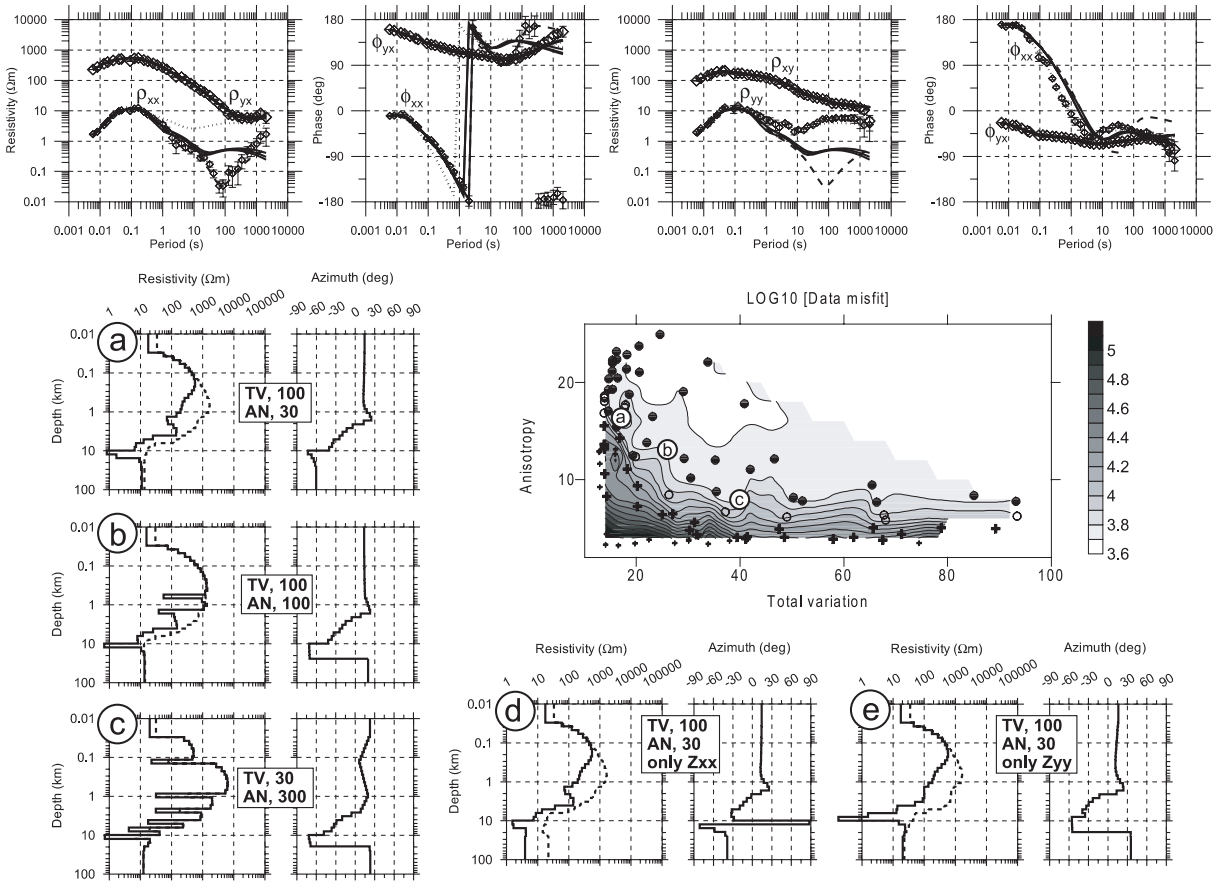

Figure 5: Inversion of practical MT data from a site situated in the transition from the South Portuguese zone to the Ossa Morena zone in southern Portugal. The solution is regularized by using the total variation and the $l1$-norm anisotropy penalties. The top panels show the experimental apparent resistivities and phases (diamonds) and the corresponding model curves for models in the subsequent panels (lines). The central right panel shows the L-surface for the penalties used. Models corresponding to the points a, b, and c are displayed in the respective panels to the left. Models d and e correspond to inversions in which only one secondary impedance was used, Z_{xx} for d (fit shown by a dashed line in the top plots) and Z_{yy} for e (dotted line in the top plots).

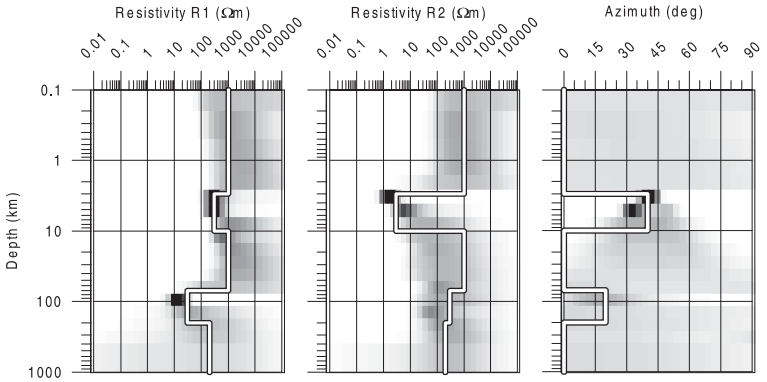

Figure 6: Inversion of the synthetic data from Section 2.3 by the MCMC method with the roughness penalty employed. The regularization parameter was 3, corresponding to weak smoothing. The gray shading visualizes a posteriori marginal conditional probability densities for the individual model parameters. The empty lines correspond to the true parameters of the underlying synthetic model.

the anisotropy strike of the deep layer show broad flat maxima around their true values, which is consistent with the pattern of the corresponding parametric sensitivities in Fig. 1.

Here, we have demonstrated the results of the MCMC inversion as a kind of postscript only to the preceding sections. It has to be emphasized, however, that this method is a stand-alone inference procedure with enormous potential in the area of geophysical inverse problems.

4 Conclusion

MT inversion for anisotropic conductivities bears some specific features as compared to isotropic models. In this contribution, we have presented a complete algorithm for a 1-D MT inversion for anisotropic layered conductors. Various regularization approaches, both quadratic and non-smooth, have been tested. The minimization of the non-linear target function is based on either the conjugate gradient reweighted optimization or on the analogy to the lagged diffusivity iterative solution. Both methods perform well with non-smooth regularizators, the former being more reliable as to the convergence, but slower than the lagged diffusivity method. The L-curve criterion allows us to objectivize the selection of optimal regularization weights, though, especially in the version for the multi-criterion regularization, the choice of the regularization parameters still depends on subjective views. The probabilistic inferring could only be demonstrated by one single example of the MCMC inversion, but the potential of this approach is rather high for anisotropic interpretations, where ambiguities and large sensitivity contrasts between different parameters largely affect the inversion procedures.

Acknowledgements

The financial support provided by the Grant Agency of the Czech Republic, through the grants No. 205/99/0917 and No. 205/01/1153, is gratefully acknowledged. Additional support was also furnished by the Ministry of Education, Youth and Sports of the Czech Republic under the contract ME185 within the Czech-Japanese Cooperation in R&D initiative. The authors would like to thank to the Academy of Sciences of the Czech Republic and ICCTI Portugal for promoting the Czech-Portuguese cooperation within the project 'Inversion of MT data using non-smooth regularization methods'.

References

Abramovici, F., 1974. The forward magnetotelluric problem for an inhomogeneous and anisotropic structure, *Geophysics*, **39**, 56–68.

Abramovici, F. and Shoham, Y., 1977. Inversion of anisotropic magnetotelluric data. *Geophys. J. R. astr. Soc.*, **50**, 55–74.

Constable, S. C., Parker, R. L. and Constable, C. G., 1987. Occam's inversion: A practical algorithm for generating smooth models from electromagnetic sounding data, *Geophysics*, **52**, 289–300.

Dekker, D. L. and Hastie, L. M., 1980. Magnetotelluric impedances of an anisotropic layered Earth model, *Geophys. J. R. astr. Soc.*, **61**, 11–20.

Eisel, M. and Haak, V., 1999. Macro-anisotropy of the electrical conductivity of the crust: A magnetotelluric study from the German Continental Deep Drilling site (KTB), *Geophys. J. Int.*, **136**, 109–122.

Engel, H. W. and Grever, W., 1994. Using the L-curve for determining optimal regularization parameters, *Numer. Math.*, **69**, 25–31.

Grandis, H., Menvielle, M. and Roussignol, M., 1999. Bayesian inversion with Markov chains - I. The magnetotelluric one-dimensional case, *Geophys. J. Int.*, **138**, 757–768.

Hansen, P. C., 1992. Analysis of discrete ill-posed problems by means of the L-curve, *SIAM Review*, **34**, 561–580.

Kováčiková, S. and Pek, J., 2002. Generalized Riccati equations for 1-D magnetotelluric impedances over anisotropic conductors, Part I: Plane wave field model, *Earth Planets Space*, 2002, in print.

Loewenthal, D. and Landisman, M., 1973. Theory for magnetotelluric observations on the surface of a layered anisotropic halfspace, *Geophys. J. R. astr. Soc.*, **35**, 195–214.

Mareschal, M., Kellett, R. L., Kurtz, R. D., Ludden, J. N. and Bailey, R. C., 1995. Archean cratonic roots, mantle shear zones, and deep electrical anisotropy, *Nature*, **373**, 134–137.

Martinez, M., 1988. Fundamentals of newer inversion procedures and their application to the 1-D inversion in the magnetotellurics, in *Proc. Coll. Electromagnetic Depth Investigations*, Haak, V. and Homilius, J. (Eds.), Univ. Frankfurt, Geol. Surv. Lower Saxony, 97–107 (in German).

Neal, R. M., 1993. Probabilistic inference using Markov chain Monte Carlo methods, *Tech. Rep. CRG-TR-93-1*, Dept. of Comp. Sci., Univ. Toronto, 140pp.

O'Brien, D. P. and Morrison, H. F., 1967. Electromagnetic fields in an N-layered anisotropic half-space, *Geophysics*, **32**, 668–677.

Pek, J. and Verner, T., 1997. Finite-difference modelling of magnetotelluric fields in two-dimensional anisotropic media, *Geophys. J. Int.*, **128**, 505–521, 1997.

Pek, J. and Santos, F. A. M., 2002. Magnetotelluric impedances and parametric sensitivites for 1-D generally anisotropic layered media, *Computers & Geosciences*, 2002, in print.

Portniaguine, O. and Zhdanov, M. S., 1999. Focusing geophysical inversion images, *Geophysics*, **64**, 874–887.

Reddy, I. K. and Rankin, D., 1971. Magnetotelluric effect of dipping anisotropies, *Geophys. Prosp.*, **19**, 84–97.

Regis, C. R. T. and Rijo, L., 1997. 1-D inversion of anisotropic magnetotelluric data, *Extended Abstracts book, 50th IC Soc. Bras. Geof. Ed.*, Brazil, vol. II, 673–674.

Regis, C. R. T. and Rijo, L., 2000. Approximate equality constraints in the inversion of anisotropic MT data, *Abstracts book, 15th Workshop on Electromagnetic Induction in the Earth*, Cabo Frio, Brazil, p. 47.

Rudin, L. L., Osher, S. and Fatemi, E., 1992. Nonlinear total variation based noise removal algorithms, *Physica D*, **60**, 259–268.

Santos, F. A. M. and Mendes-Victor, L. A., 1997. 1-D interpretation of anisotropic MT data, *Extended Abstracts book, 50th IC Soc. Bras. Geof. Ed.*, Brazil, vol. II, 772–775.

Santos, F. A. M., Pous, J., Almeida, E. P., Queralt, P., Marcuello, A., Matias H. and Mendes-Victor, L. A., 1999. Magnetotelluric survey of the electrical conductivity of the crust across the Ossa Morena Zone and South Portuguese Zone suture, *Tectonophysics*, **313**, 449–462.

Tikhonov, A. N. and Arsenin, V. Y., 1997. *Solution of ill-posed problems*, W. H. Winston and Sons, Washington D. C.

Vogel, C. R. and Oman, M. E., 1998. Fast, robust total variation-based reconstruction of noisy, blurred images, *IEEE Trans. Image Proc.*, **7**, 813–824.